

High-temperature molecular beam epitaxy of hexagonal boron nitride layers

Tin S. Cheng, Alex Summerfield, Christopher J. Mellor, Andrew Davies, Andrei N. Khlobystov, Laurence Eaves, C. Thomas Foxon, Peter H. Beton, and Sergei V. Novikov

Citation: *Journal of Vacuum Science & Technology B, Nanotechnology and Microelectronics: Materials, Processing, Measurement, and Phenomena* **36**, 02D103 (2018); doi: 10.1116/1.5011280

View online: <https://doi.org/10.1116/1.5011280>

View Table of Contents: <http://avs.scitation.org/toc/jvb/36/2>

Published by the [American Vacuum Society](#)

Articles you may be interested in

[Predicting synergy in atomic layer etching](#)

Journal of Vacuum Science & Technology A: Vacuum, Surfaces, and Films **35**, 05C302 (2017); 10.1116/1.4979019

[Innovative metallic solutions for alpine ski bases](#)

Journal of Vacuum Science & Technology B, Nanotechnology and Microelectronics: Materials, Processing, Measurement, and Phenomena **36**, 01A108 (2018); 10.1116/1.5002542

[Surface and interface properties of polar thin films on a ferroelectric substrate: ZnO on LiNbO₃ \(0001\) and \(000 \$\bar{1}\$ \)](#)

Journal of Vacuum Science & Technology A: Vacuum, Surfaces, and Films **36**, 021511 (2018); 10.1116/1.5012762

[Novel plasma enhanced chemical vapor deposition of highly conformal SiN films and their barrier properties](#)


Journal of Vacuum Science & Technology B, Nanotechnology and Microelectronics: Materials, Processing, Measurement, and Phenomena **36**, 022201 (2018); 10.1116/1.5002660

[Growth of high-quality Bi₂Se₃ topological insulators using \(Bi_{1-x}In_x\)₂Se₃ buffer layers](#)

Journal of Vacuum Science & Technology B, Nanotechnology and Microelectronics: Materials, Processing, Measurement, and Phenomena **36**, 02D101 (2018); 10.1116/1.5015968

[Silicon-carbon composites for lithium-ion batteries: A comparative study of different carbon deposition approaches](#)

Journal of Vacuum Science & Technology B, Nanotechnology and Microelectronics: Materials, Processing, Measurement, and Phenomena **36**, 011402 (2018); 10.1116/1.5006220



Instruments for Advanced Science

Contact Hiden Analytical for further details:
www.HidenAnalytical.com
info@hiden.co.uk

CLICK TO VIEW our product catalogue



Gas Analysis

- dynamic measurement of reaction gas streams
- catalysis and thermal analysis
- molecular beam studies
- dissolved species probes
- fermentation, environmental and ecological studies



Surface Science

- UHV TPD
- SIMS
- end point detection in ion beam etch
- elemental imaging - surface mapping



Plasma Diagnostics

- plasma source characterization
- etch and deposition process reaction kinetic studies
- analysis of neutral and radical species



Vacuum Analysis

- partial pressure measurement and control of process gases
- reactive sputter process control
- vacuum diagnostics
- vacuum coating process monitoring

High-temperature molecular beam epitaxy of hexagonal boron nitride layers

Tin S. Cheng, Alex Summerfield, and Christopher J. Mellor

School of Physics and Astronomy, University of Nottingham, Nottingham NG7 2RD, United Kingdom

Andrew Davies

School of Physics and Astronomy and School of Chemistry, University of Nottingham, Nottingham NG7 2RD, United Kingdom

Andrei N. Khlobystov

School of Chemistry, University of Nottingham, Nottingham NG7 2RD, United Kingdom

Laurence Eaves, C. Thomas Foxon, Peter H. Beton, and Sergei V. Novikov^{a)}

School of Physics and Astronomy, University of Nottingham, Nottingham NG7 2RD, United Kingdom

(Received 31 October 2017; accepted 17 January 2018; published 9 February 2018)

The growth and properties of hexagonal boron nitride (hBN) have recently attracted much attention due to applications in graphene-based monolayer thick two dimensional (2D)-structures and at the same time as a wide band gap material for deep-ultraviolet device (DUV) applications. The authors present their results in the high-temperature plasma-assisted molecular beam epitaxy (PA-MBE) of hBN monolayers on highly oriented pyrolytic graphite substrates. Their results demonstrate that PA-MBE growth at temperatures $\sim 1390^\circ\text{C}$ can achieve mono- and few-layer thick hBN with a control of the hBN coverage and atomically flat hBN surfaces which is essential for 2D applications of hBN layers. The hBN monolayer coverage can be reproducibly controlled by the PA-MBE growth temperature, time and B:N flux ratios. Significantly thicker hBN layers have been achieved at higher B:N flux ratios. The authors observed a gradual increase of the hBN thickness from 40 to 70 nm by decreasing the growth temperature from 1390 to 1080°C . However, by decreasing the MBE growth temperature below 1250°C , the authors observe a rapid degradation of the optical properties of hBN layers. Therefore, high-temperature PA-MBE, above 1250°C , is a viable approach for the growth of high-quality hBN layers for 2D and DUV applications. © 2018 Author(s). All article content, except where otherwise noted, is licensed under a Creative Commons Attribution (CC BY) license (<http://creativecommons.org/licenses/by/4.0/>).

<https://doi.org/10.1116/1.5011280>

I. INTRODUCTION

The growth and properties of hexagonal boron nitride (hBN) have recently attracted much attention. There are two main reasons for this high level of activity. First, the lattice parameter of hBN is very close to that of the graphene.¹ The surface of hBN is atomically flat and can provide an ideal chemically inert dielectric substrate for atomically thin mono- and few-layer 2D-structures.^{2–7} hBN can also act as an insulating barrier or, when it is only a few atomic layers thick, as a tunnel barrier for electrons in 2D-structures.^{3,4,6} Second, the band gap of hBN is large, $\sim 6\text{eV}$, and this has fueled interest in hBN as a wide gap material for deep-ultraviolet device (DUV) applications.^{8,9} The development of group III nitrides allows researchers worldwide to consider AlGaN based light emitting diodes as a possible new alternative DUV light source for water purification and surface decontamination. Hexagonal boron nitride has a potential advantage over AlGaN in such DUV structures due to the possibility of more efficient *p*- and *n*-doping.^{8,9}

Currently, there is no reliable technology able to provide large area hBN bulk single crystals. Research on the growth of bulk hBN single crystals is limited due to the high melting temperature of boron and the low solubility of nitrogen in

liquid boron. Therefore, the growth of bulk BN has been studied using an alternative solvent solution.^{10–18} To date, the highest structural quality hBN bulk crystals have been achieved by a high-temperature high-pressure growth method.^{15–17} The size of hBN bulk crystals still remains very small, less than a few millimeters in diameter. However, due to the high structural quality and good optical properties, hBN flakes exfoliated from these bulk crystals are now widely used as substrates for the growth and manufacture of 2D-structures.^{2–7}

Recently, there have been many attempts to develop a reproducible technology for the growth of large area boron nitride layers by chemical vapor deposition,^{19–21} metal-organic chemical vapor deposition^{8,9,22} and molecular beam epitaxy (MBE).^{23–38} Progress in MBE growth of boron nitride layers has been relatively slow, partly due to a lack of an efficient MBE source for boron, due to its very low vapor pressure.

We have recently demonstrated growth of hBN layers using plasma-assisted molecular beam epitaxy (PA-MBE) at very high growth temperatures from 1390 to 1690°C .³³ Atomic force microscopy (AFM) measurements show mono- and few-layer hBN island growth. Our conducting AFM measurements on the electrical resistivity of MBE-grown hBN monolayers^{33,39} is consistent with earlier measurements on monolayers, exfoliated from high quality bulk

^{a)}Electronic mail: Sergei.Novikov@nottingham.ac.uk

hBN crystals.^{4,15} The high optical quality of our hBN grown at high temperatures on highly oriented pyrolytic graphite (HOPG) has been confirmed by both spectroscopic ellipsometry and photoluminescence spectroscopy.^{33,37} Using AFM we also observe hexagonal moiré patterns, consistent with the close rotational alignment of the hBN lattice and the graphite substrate.^{33,39}

In this paper, we present our recent results on the high-temperature PA-MBE growth of hBN monolayers with atomically controlled thicknesses for 2D applications and on the growth of significantly thicker hBN layers for potential DUV applications.

II. EXPERIMENT

The growth of hBN layers was performed using a custom-designed, dual chamber GENxplor MBE system modified to achieve growth temperatures of up to 1850 °C under ultrahigh vacuum conditions on rotating substrates of up to 3 in. in diameter. Details of the MBE system are described elsewhere.⁴⁰ In this study, we use thermocouple readings to measure the substrate temperature.^{33,37,40} We have used a high-temperature Veeco effusion cell for sublimation of boron and a standard Veeco radio-frequency (RF) plasma source for active nitrogen. Boron has two naturally occurring stable isotopes, ¹¹B (80.1%) and ¹⁰B (19.9%).⁴¹ In our MBE growth, we have used high-purity (5N) elemental boron, which contains this natural mixture of these isotopes.

All hBN layers investigated in this paper were grown using the nitrogen (N₂) flow of 2 sccm and a fixed RF power of 550 W. We performed the growth on 10 × 10 mm² HOPG substrates with a mosaic spread of 0.4°. Before introduction into the MBE growth chamber, the HOPG substrates were cleaned by exfoliation using adhesive tape to obtain a fresh HOPG surface for growth. Following exfoliation, the HOPG substrates were further cleaned in toluene and annealed at 200 °C in H₂:Ar gas flow, as previously described.^{33,37}

The structural properties of the BN layers were studied *in situ* using reflection high-energy electron diffraction (RHEED) and after growth *ex situ* measurements were performed using x-ray diffraction (XRD).

Images of the hBN layers after growth were acquired with both amplitude-modulated tapping mode AFM (AC-AFM) in repulsive mode and contact mode AFM under ambient conditions using an Asylum Research Cypher-S AFM and Multi75A1-G (Budget Sensors, stiffness ~3 N/m) cantilevers. AFM image processing and analysis was performed using Gwyddion.

Variable angle spectroscopic ellipsometry was carried out using a M2000-DI instrument made by J.A. Woollam, Inc. The results were obtained over a wavelength range from 1690 to 192 nm using focussing probes resulting in an elliptical spot with a minor axis of 200 μm; the major axis of the ellipse depends on the angles of incidence, which were 55°, 60°, and 65°. Analysis was carried out using CompleteEase version 5.19. The mosaic spread of the HOPG substrate means that we need to allow for an angular offset in the ellipsometric models. When measuring thin layers (<10 nm)

this leads to additional uncertainties in fitted parameter values.

The chemical concentrations of B and N were studied as a function of depth using secondary ion mass spectrometry (SIMS) in a Cameca IMS-3F system. The analysis of the samples was carried out using O₂⁺ primary ion bombardment and positive secondary ion detection of the ¹⁰B isotope to optimize sensitivity to boron.

III. RESULTS AND DISCUSSION

For 2D applications of boron nitride, it is important to develop the MBE technology of mono- and few-layer hBN with atomically flat surfaces and monolayer control of the thickness. We have already demonstrated that we can control the hBN layer coverage by adjusting the epitaxial growth temperatures for submonolayer thicknesses.^{33,37} Several hBN layers were grown under the same B and active nitrogen fluxes on sapphire and HOPG substrates in the temperature range from 1390 to 1690 °C.³⁷ At the highest growth temperatures, only a small density of hBN islands was observed and the coverage gradually increased to a complete hBN monolayer by decreasing the growth temperature. This effect has been explained by hBN sublimation at high MBE growth temperatures above 1390 °C.³⁷

Another way to control reproducibly the hBN monolayer coverage is to change the MBE growth time. Figure 1 presents AFM images of the hBN islands grown at 1390 °C on HOPG surface for fixed boron and nitrogen fluxes as a function of the deposition time. The upper row [(a)–(c)] shows topographic AC-AFM images, and the bottom row shows the corresponding phase-channel images [(d)–(f)], which highlights clearly the hBN islands and exposed HOPG regions.

After 1 h of growth, we observe a high density of hexagonal hBN islands nucleating on the HOPG, as shown in Figs. 1(a) and 1(d). The nucleation points are primarily along the step-edges of HOPG; however, there is also a high density of hBN hexagons on the HOPG plates. With increasing the growth time to 3 h, it is possible to observe coalescence of the hBN islands and formation of one hBN monolayer, as shown in Figs. 1(b) and 1(e). There are still small areas of the open uncoated HOPG surface, as indicated in Fig. 1(e), so the hBN coverage is still slightly below 1 ML. The surface of coalesced hBN is atomically flat. One can also observe the formation of the second and third hBN monolayers along the HOPG step edges. With the further increase of the growth time up to 5 h, we can achieve complete coalescence and complete coverage of hBN which is shown in Figs. 1(c) and 1(f). However, at this stage we also observe the formation of three-dimensional (3D) material growth on the surface, partially due to the twist between HOPG plates. Figure 1 clearly demonstrates that by controlling the growth time this allows us to control the hBN growth coverage and to achieve atomically flat hBN surfaces.

We observe a streaky RHEED pattern on the HOPG wafers at room temperature and after heating to growth temperature, as shown in Fig. 2(a). HOPG substrates have

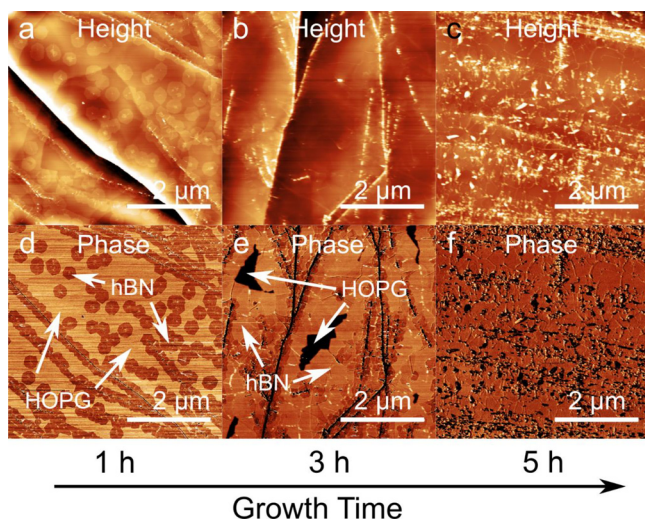


FIG. 1. (Color online) AC-AFM images of hBN growth on HOPG with $T_B = 1875^\circ\text{C}$ for increasing growth time at a substrate temperature of 1390°C . (a) Height image of hBN growth after 1 h. (b) Height image of hBN growth after 3 h. (c) Height image of hBN growth after 5 h. [(d)–(f)] Phase images for the height images (a)–(c), respectively. The arrows in (d) and (e) indicate regions of hBN growth and exposed HOPG, while for (c) and (f) the surface is completely covered by hBN growth.

randomly oriented domains, twisted with respect to each other. All the domains have atomically flat surfaces. Therefore, on HOPG, we record a streaky RHEED pattern for all azimuthal directions of the primary beam. We did not observe any significant change in the RHEED pattern after the start of the growth of monolayer thick boron nitride. The RHEED remains streaky, which confirms the flat morphology of the monolayer thick hBN film. The lattice mismatch between hBN and HOPG is very small and is only $\sim 1.8\%$ for the a -parameter.^{1,42} Therefore, the absence of any extra streaks or of widening of the RHEED streaks confirms flat surface of hBN layers and good rotational alignment of the hBN layer and the graphite domains.

Figure 3 shows absorption coefficient spectra calculated from spectroscopic ellipsometric measurements made on two hBN samples grown on HOPG for 1 and 5 h. For these samples, the fact that the focussing probes increase the acceptance angle for the reflected light allows the light reflected from the HOPG polycrystals to be collected in spite of the angular spread around the surface normal.³⁷ The

optical model of the HOPG substrate was determined by measuring the back surface of one of the samples. The sharp increase in absorption for both samples indicates a band-gap at around 5.7 eV , similar to that of high-quality bulk hBN.¹³ For the sample grown for 1 h, the layer thickness of 0.35 nm was measured by AFM. Using the submonolayer coverage determined by AFM, a Bruggeman effective medium approximation is used to estimate the optical response of the hBN islands. The optical response is modeled as a single Gaussian oscillator with a UV pole. An additional constraint is used to ensure that the model is reasonable: the hBN refractive index is around 1.6 at a photon energy close to 2 eV . The hBN layer grown for 5 h is found to have a thickness of $2.9 \pm 0.9\text{ nm}$ (determined as an average value over the measurement ellipse). At the longer growth time of 5 h, the absorption spectrum displays a broader absorption feature that extends to lower energies, possibly arising from greater inhomogeneity due to the beginning of 3D island formation, as shown in Fig. 1.

The data shown in Fig. 3 uses an average film thickness that was determined by AFM. This AFM data was necessarily taken over a much smaller and different area than the ellipsometry measurement, so we cannot rule out the possibility that part of the difference in the magnitude of the absorption coefficient is due to uncertainty as to the thickness of the film. The hBN layer grown for 1 h has submonolayer coverage, as shown in Figs. 1(a) and 1(d) and AFM suggests that the islands might be expected to be reasonably good single crystals, whereas the 5 h growth results in a layer that has an average thickness of more than one monolayer and will include domain boundaries and regions, where the film will have other defects [Figs. 1(c) and 1(f)]. Therefore, the absorption coefficient might be affected by inhomogeneous broadening and parts of the film (e.g., at domain boundaries) might be less efficient at absorbing light than in an ensemble of single crystals. Both effects will reduce the absorption coefficient for the thicker hBN layer.

Figure 4 presents another way to control the MBE growth of hBN layers by increasing the temperature of the boron sublimation source (T_B). These hBN layers were grown at 1390°C on HOPG substrates with a fixed active nitrogen flux. An increase in the temperature of the boron source results in an increase of the boron flux coming to the growth

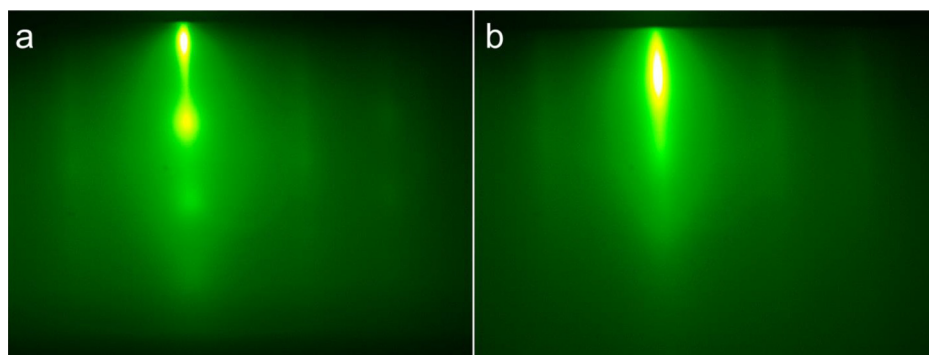


FIG. 2. (Color online) RHEED patterns of the HOPG substrate and the hBN layer at a growth temperature of 1390°C : (a) HOPG before the start of hBN growth; (b) during the growth of hBN with a boron cell temperature $T_B = 1925^\circ\text{C}$ after a growth time of 2 h.

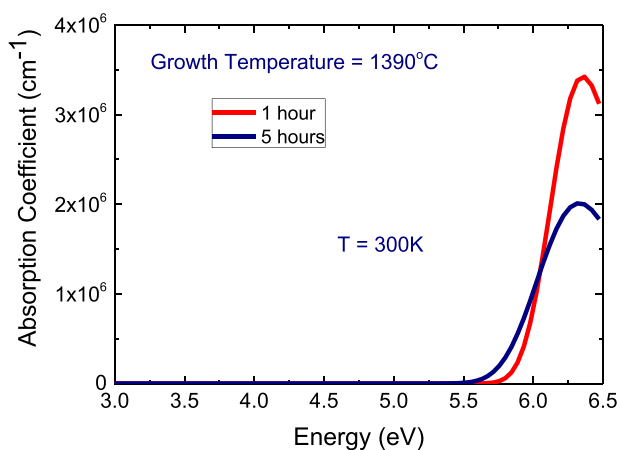


Fig. 3. (Color online) Room temperature absorption coefficients as a function of photon energy for two of the hBN layers grown for 1 and 5 h at a substrate temperature of 1390 °C and $T_B = 1875$ °C. The absorption coefficients are calculated from the results of variable angle spectroscopic ellipsometer measurements. The optical model consists of a single Gaussian oscillator and a UV pole, the model also allows for an offset to the angle of incidence to take account of the mosaic spread of the HOPG.

surface and therefore an increase in the hBN growth rate. In Fig. 4 we quote the temperatures of the boron cell, but not the boron beam equivalent pressures (BEP), because we were not able to achieve reliable measurements of the boron flux with the beam monitoring ion gauge. At extremely high source temperatures above 1800 °C, the boron source produces not only a flux of boron, but also a flux of nitrogen, due to the start of sublimation of the BN components of the cell. Therefore, we were not able to reliably measure boron BEP data. With the increase of the boron flux we can achieve complete hBN coverage faster, as can be seen by comparing AFM images of the hBN surface in Figs. 4(a) and 4(b). However, with further increase in the boron flux, we start to observe 3D island growth, as shown in Figs. 4(c) and 4(d). This is probably a result of a change in the B to active nitrogen flux ratio at the growth interface, which produces the excess boron on the surface, responsible for the observed 3D growth. However, it may be that with a natural progression

the growth becomes more 3D as the step edges coalesce and cover the surface. The further increase of the boron source temperature resulted in even rougher surfaces.

The RHEED pattern remains streaky during growth of the hBN layers presented in Fig. 4. Figure 2(b) shows the RHEED pattern during the growth of the hBN layer at a temperature of 1390 °C with the boron cell $T_B = 1925$ °C. The streaky RHEED confirms the flat morphology of the grown hBN film and good rotational alignment of the hBN layer and the graphite domains. These results demonstrate that high-temperature PA-MBE can achieve growth of mono- and few-layer hBN with a control of the hBN coverage, as well as atomically flat hBN surfaces which is essential for 2D applications of hBN layers.

However, for DUV applications of hBN, we need to be able to achieve significantly thicker hBN layers with thicknesses of tens or hundreds of nanometers. In order to increase the hBN thickness in MBE one needs to be able to increase the fluxes of both boron and the active nitrogen. We are currently using a high-temperature effusion source for boron sublimation. In the experiments described below we have studied the high-temperature MBE growth of hBN with higher boron fluxes by increasing the boron cell temperatures to 1975 °C. Figure 5 shows the dependence of the thickness of hBN layers against the growth temperature. All layers were grown under the same boron and active nitrogen fluxes for 3 h. The thickness of the layers were measured by variable angle spectroscopic ellipsometry. We demonstrated previously that the hBN coverage increases with decreasing MBE growth temperatures from 1690 to 1390 °C due to the decrease in re-evaporation of boron from the growth surface.³⁷ Figure 5 presents results for a significantly lower growth temperature range from 1390 to 1080 °C and at the higher boron flux values. We observed a gradual increase of the hBN thickness from 40 to 70 nm by decreasing the growth temperature from 1390 to 1080 °C. The increase must be attributed to increase in the boron concentration at the growth surface due to a decrease in the boron re-evaporation, which becomes negligible for the temperatures below 1000 °C.^{43,44}

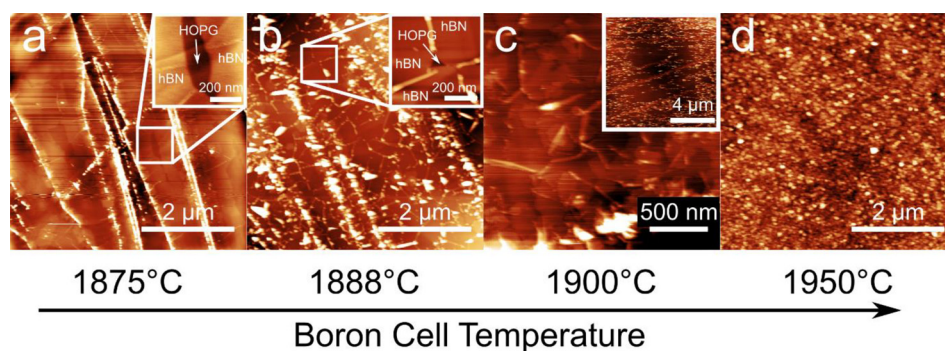


Fig. 4. (Color online) AFM data for hBN growth on HOPG for increasing boron flux [increasing B cell temperature (T_B)] at a fixed MBE growth time of 3 h and temperature of 1390 °C. (a) AC-AFM image of hBN on HOPG at $T_B = 1875$ °C. (inset) Image of the region indicated by the white box showing the coalescence of hBN growth with an exposed central region of HOPG. (b) AC-AFM image of hBN growth with $T_B = 1888$ °C. (inset) Image of the region indicated by the white box in (b) showing a small triangular region of exposed HOPG surrounded by hBN domains. (c) Contact-AFM image of hBN growth for $T_B = 1900$ °C showing multilayer hBN growth. (inset) Large-area image of the region in c, showing material swept aside by the AFM tip during contact-AFM imaging. (d) AC-AFM image of hBN growth for $T_B = 1950$ °C showing complete coverage of HOPG with granular hBN deposits.

The XRD spectra of the thicker hBN layers were dominated by strong peaks from the HOPG substrate. The lattice constants of graphite and hBN are very close^{1,42} and the thicknesses of our hBN layers are still a few tens of nanometers. Therefore, we were not able to resolve any new extra XRD peaks related to the hBN layers within the sensitivity of our XRD system.

SIMS boron profiles for two hBN samples grown at different MBE temperatures are shown in Fig. 6. It was found that the roughness of clean HOPG wafers exceeded the depth of the sputtered SIMS craters, making it impossible to obtain accurate crater depth measurements using a profilometer. Therefore, the ¹⁰B isotope SIMS profiles are plotted in Fig. 6 as a function of the sputtering time. The difference in the boron concentration for two layers is mainly due to low accuracy of the SIMS measurements for such nanometer thick layers. Figure 6 demonstrates an increase of the SIMS sputtering time required to reach the BN/graphite interface with decreasing growth temperature. This confirms the results of Fig. 5, that the hBN layers grown under the same MBE conditions become thicker when they are grown at lower temperatures. As discussed above, the boron sticking coefficient at MBE temperatures below 1000 °C is close to 1. All arriving boron atoms stick and remain on the growth surface. The increase in the thickness of hBN with decrease of the growth temperature below 1300 °C must be attributed to the increase in the sticking coefficient of boron and therefore increase in the boron concentration at the growth surface due to a decrease in the boron re-evaporation. From our experience in PA-MBE with different types of the RF nitrogen plasma sources for the growth of Ga(Al)N layers,⁴⁵ we expect that active nitrogen flux produced by the standard Veeco RF source used in this work will allow us to achieve GaN growth rates of $\sim 0.2 \mu\text{m/h}$ at temperatures $\sim 750^\circ\text{C}$. Thicknesses of hBN layers grown at $\sim 1080^\circ\text{C}$ as shown in Fig. 5 are significantly lower, even if we take into account difference in lattice constants of GaN and hBN. Therefore,

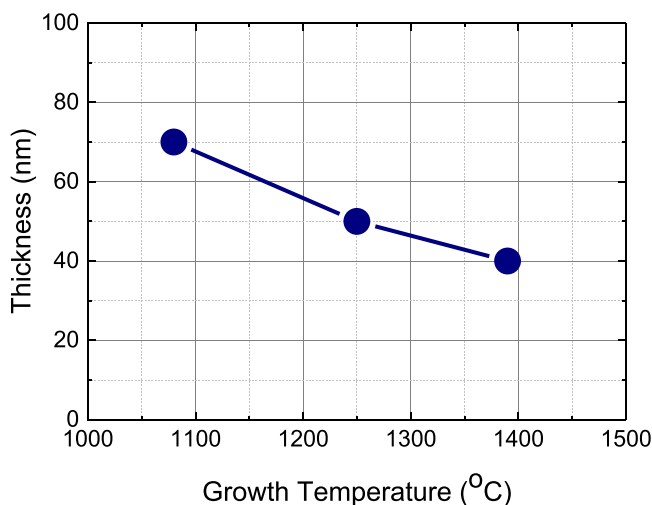


Fig. 5. (Color online) Thickness of BN layers grown at different growth temperatures determined by variable angle spectroscopic ellipsometry. The growth time for these hBN layers was 3 h.

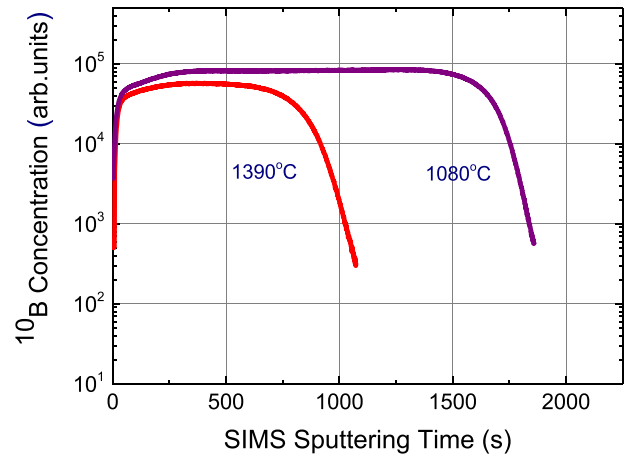


Fig. 6. (Color online) SIMS ¹⁰B isotope profiles for two BN samples grown at different growth temperatures.

the hBN layers, shown in Fig. 5, were grown under a high excess of active nitrogen species.

Figure 7 shows absorption coefficient spectra obtained from spectroscopic ellipsometric measurements made on the three hBN layers, grown on HOPG at a different growth temperatures. The thicknesses of the layers are shown in Fig. 5. All three samples show significant absorption above 4.0 eV, in contrast to data from the thin hBN samples grown at lower boron flux of 1875 °C and at the growth temperature of 1390 °C, shown in Fig. 3. The sharp increase in absorption for the sample grown at the highest temperature of 1390 °C indicates a bandgap at around 5.7 eV, similar to the high-quality thin hBN, shown in Fig. 3. With the decrease of the growth temperature to 1250 °C, we can see that a low energy defect band below 5.5 eV has developed with an increase in absorption around 4.5 eV, suggesting an increase in the density of the point defects in the hBN layer. With the further decrease of the growth temperature to 1080 °C, one can

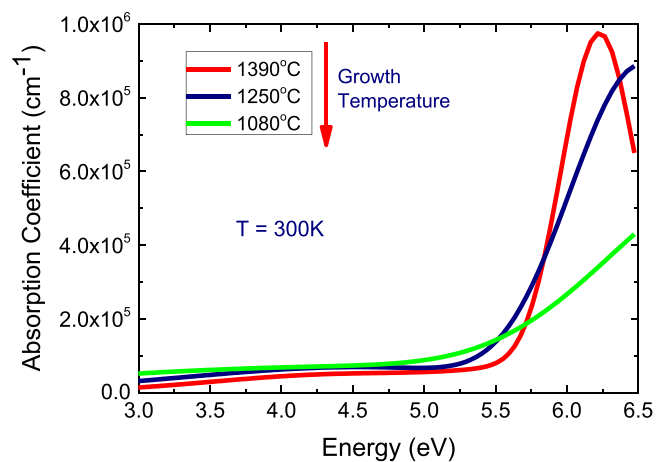


Fig. 7. (Color online) Optical absorption coefficients for three hBN layers grown at different growth temperatures determined from variable angle spectroscopic ellipsometer measurements. The thicknesses of these layers are shown in Fig. 5. The optical model consisted of two Gaussian oscillators (three for the sample grown at 1390 °C) and a UV pole. One of the Gaussian oscillators describes the response due to the band gap of the hBN, the other oscillator(s) describes the tail that extends to lower energies.

observe further broadening of the absorption around 6 eV as well as an increase in the range of energies associated with defect absorption around 4.5 eV, demonstrating degradation of the optical properties of hBN layers as the growth temperature is reduced. It is important to note that the maximum growth temperature of standard MBE systems range from about 700 to 900 °C. Therefore, it seems unlikely that hBN layers with good optical properties can be grown with standard MBE systems and only high-temperature systems with growth temperatures above ~1250 °C, are a more viable MBE approach for the growth of high-quality hBN layers.

IV. SUMMARY AND CONCLUSIONS

Our results demonstrate that PA-MBE at growth temperatures of ~1390 °C can achieve mono- and few-layer thick hBN with a control of the hBN coverage and atomically flat hBN surfaces. The hBN monolayer coverage can be reproducibly controlled by the PA-MBE growth temperature, time, and B:N flux ratios. Significantly thicker hBN layers have been achieved at the higher B:N flux ratios. With the decrease of the PA-MBE growth temperature below 1250 °C we observe rapid degradation of the optical properties of hBN layers.

ACKNOWLEDGMENTS

This work was supported by the Engineering and Physical Sciences Research Council UK [Grant Nos. EP/K040243/1, EP/L013908/1, EP/P019080/1, EP/M013294/1, and EP/M50810X/1]; and Leverhulme Trust [Grant No. RPG-2014-129]. The authors acknowledge Loughborough Surface Analysis, Ltd., for SIMS measurements and discussions of the results.

¹C. R. Woods *et al.*, *Nat. Phys.* **10**, 451 (2014).

²C. R. Dean *et al.*, *Nat. Nanotechnol.* **5**, 722 (2010).

³L. Britnell, R. V. Gorbachev, A. K. Geim, L. A. Ponomarenko, A. Mishchenko, M. T. Greenaway, T. M. Fromhold, K. S. Novoselov, and L. Eaves, *Nat. Commun.* **4**, 1794 (2013).

⁴L. Britnell *et al.*, *Nano Lett.* **12**, 1707 (2012).

⁵W. Yang *et al.*, *Nat. Mater.* **12**, 792 (2013).

⁶L. Britnell *et al.*, *Science* **335**, 947 (2012).

⁷S. Tang *et al.*, *Nat. Commun.* **6**, 6499 (2015).

⁸H. X. Jiang and J. Y. Lin, *Semicond. Sci. Technol.* **29**, 084003 (2014).

⁹H. X. Jiang and J. Y. Lin, *ECS J. Solid State Sci. Technol.* **6**, Q3012 (2017).

¹⁰T. Ishii and T. Sato, *J. Cryst. Growth* **61**, 689 (1983).

¹¹M. Hubacek and T. Sato, *J. Mater. Sci.* **32**, 3293 (1997).

¹²M. Yano, M. Okamoto, Y. K. Yap, M. Yoshimura, Y. Mori, and T. Sasaki, *Diamond Relat. Mater.* **9**, 512 (2000).

¹³K. Watanabe, T. Taniguchi, and H. Kanda, *Nat. Mater.* **3**, 404 (2004).

¹⁴Y. Gu, M. Zheng, Y. Liu, and Z. Xu, *J. Am. Ceram. Soc.* **90**, 1589 (2007).

¹⁵T. Taniguchi and K. Watanabe, *J. Cryst. Growth* **303**, 525 (2007).

¹⁶Y. Kubota, K. Watanabe, O. Tsuda, and T. Taniguchi, *Science* **317**, 932 (2007).

¹⁷K. Watanabe and T. Taniguchi, *Phys. Rev. B* **79**, 193104 (2009).

¹⁸J. H. Edgar, T. B. Hoffman, B. Clubine, M. Currie, X. Z. Du, J. Y. Lin, and H. X. Jiang, *J. Cryst. Growth* **403**, 110 (2014).

¹⁹L. Song *et al.*, *Nano Lett.* **10**, 3209 (2010).

²⁰K. K. Kim *et al.*, *Nano Lett.* **12**, 161 (2012).

²¹S. Caneva *et al.*, *Nano Lett.* **15**, 1867 (2015).

²²X. Li *et al.*, *Sci. Rep.* **7**, 786 (2017).

²³M. J. Paisley, Z. Sitar, B. Van, and R. F. Davis, *J. Vac. Sci. Technol., B* **8**, 323 (1990).

²⁴V. K. Gupta, C. C. Wamsley, M. W. Koch, and G. W. Wicks, *J. Vac. Sci. Technol., B* **17**, 1246 (1999).

²⁵C. L. Tsai, Y. Kobayashi, T. Akasaka, and M. Kasu, *J. Cryst. Growth* **311**, 3054 (2009).

²⁶K. Hirama, Y. Taniyasu, S. Karimoto, Y. Krockenberger, and H. Yamamoto, *Appl. Phys. Lett.* **104**, 092113 (2014).

²⁷Z. Xu, R. Zheng, A. Khanaki, Z. Zuo, and J. Liu, *Appl. Phys. Lett.* **107**, 213103 (2015).

²⁸S. Nakhaie, J. M. Wofford, T. Schumann, U. Jahn, M. Ramsteiner, M. Hanke, J. M. J. Lopes, and H. Riechert, *Appl. Phys. Lett.* **106**, 213108 (2015).

²⁹Z. Zuo, Z. Xu, R. Zheng, A. Khanaki, J.-G. Zheng, and J. Liu, *Sci. Rep.* **5**, 14760 (2015).

³⁰A. T. Barton *et al.*, *Microelectron. Eng.* **147**, 306 (2015).

³¹A. A. Tonkikh, E. N. Voloshina, P. Werner, H. Blumtritt, B. Senkovskiy, G. Güntherodt, S. S. P. Parkin, and Yu. S. Dedkov, *Sci. Rep.* **6**, 23547 (2016).

³²Z. Xu, A. Khanaki, H. Tian, R. Zheng, M. Suja, J.-G. Zheng, and J. Liu, *Appl. Phys. Lett.* **109**, 043110 (2016).

³³Y. J. Cho *et al.*, *Sci. Rep.* **6**, 34474 (2016).

³⁴J. M. Wofford, S. Nakhaie, T. Krause, X. Liu, M. Ramsteiner, M. Hanke, H. Riechert, and J. M. J. Lopes, *Sci. Rep.* **7**, 43644 (2017).

³⁵Z. Xu, H. Tian, A. Khanaki, R. Zheng, M. Suja, and J. Liu, *Sci. Rep.* **7**, 43100 (2017).

³⁶K. Hirama, Y. Taniyasu, S. Karimoto, H. Yamamoto, and K. Kumakura, *Appl. Phys. Express* **10**, 035501 (2017).

³⁷T. Q. P. Vuong *et al.*, *2D Mater.* **4**, 021023 (2017).

³⁸A. Khanaki, Z. Xu, H. Tian, R. Zheng, Z. Zuo, J. G. Zheng, and J. Liu, *Sci. Rep.* **7**, 4087 (2017).

³⁹A. Summerfield *et al.*, "Moiré-modulated conductance of hexagonal boron nitride tunnel barriers" (unpublished).

⁴⁰T. S. Cheng *et al.*, *J. Vac. Sci. Technol., B* **34**, 02L101 (2016).

⁴¹National Institute of Standards and Technology, "Atomic weights and isotopic compositions for all elements," https://physics.nist.gov/cgi-bin/Compositions/stand_alone.pl.

⁴²W. Paszkowicz, J. B. Pelka, M. Knapp, T. Szyszko, and S. Podsiadlo, *Appl. Phys. A* **75**, 431 (2002).

⁴³"MBE Technologies," <http://www.veeco.com/technologies-and-products/mbe-technologies>.

⁴⁴R. E. Honig and D. A. Kramer, *RCA Rev.* **30**, 285 (1969).

⁴⁵S. V. Novikov, A. J. Kent, and C. T. Foxon, *Prog. Cryst. Growth Charact. Mater.* **63**, 25 (2017).